Journal of Organometallic Chemistry, 319 (1987) 265–283
Elsevier Sequoia S.A., Lausanne – Printed in The Netherlands

MOLECULAR ORBITAL ANALYSIS OF THE BONDING IN PLATINUM PHOSPHINE HYDRIDE CLUSTERS

DAVID G. EVANS

Department of Chemistry, University of Exeter, Stocker Road, Exeter, EX4 4QD (Great Britain)

(Received August 12th, 1986)

Summary

The electronic and structural features of platinum clusters containing tertiary phosphine and hydride ligands have been analysed using Extended Hückel molecular orbital calculations. The calculations illustrate how the non-conical nature of the constituent PtL_2 fragments leads to their having a marked conformational preference in the clusters. The introduction of PtL fragments into some of the clusters leads to a further flexibility in electron count which may also be rationalised on the basis of the analysis presented here.

In recent years Spencer et al. [1–3] have reported a fascinating series of platinum phosphine hydride clusters of general formula $Pt_x(PR_3)_yH_z^{n+}$, which show considerable flexibility in their number of cluster bonding electrons and metal core geometry. In an earlier paper [4] we developed a molecular orbital analysis of the bonding in some members of this series and showed how their electronic and structural features could be interpreted in terms of the bonding capabilities of the angular PtL_2 fragment. It is the purpose of this paper to extend this theoretical analysis to encompass new members of the series reported [3] since our previous work [4] was published. Our analysis is based on elementary symmetry and perturbation theory arguments supported by Extended Hückel molecular orbital calculations [5] with the parameters given in the Appendix.

Whilst the bonding in clusters derived from conical $M(CO)_3$ and $M(C_5H_5)$ fragments is well understood and may be described in terms of the Polyhedral Skeletal Electron Pair Theory [6] based on the isolobal relationship [7] between these fragments and BH, significant differences are apparent for clusters containing PtL_2 fragments. A comparison of the frontier molecular orbitals of $M(CO)_3$ and PtL_2 fragments (see Fig. 1) [8], shows that although both fragments have similar hy(s-z) and hy(xz) outpointing orbitals suitable for skeletal bonding, the hy(yz) orbital of $M(CO)_3$ is replaced by a lower lying d_{yz} and a much higher lying p_y

0022-328X/87/$03.50

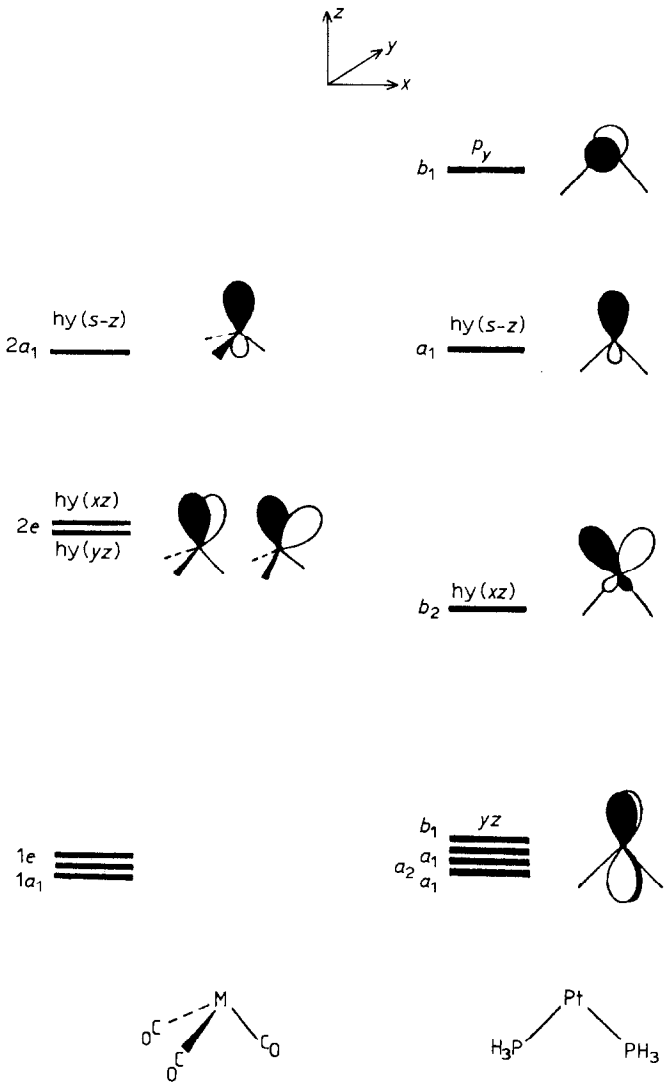

Fig 1. A comparison of the frontier MOs of $M(CO)_3$ and $Pt(PH_3)_2$ fragments.

orbital in the PtL_2 fragment. The overlap between d_{yz} orbitals on adjacent metal atoms is too small to make a significant contribution to the total metal–metal bonding and gives rise to a closely spaced set of occupied orbitals within the cluster. The overlap between p_y orbitals on adjacent metal atoms is large however and therefore the hy(s-z), hy(xz) and p_y orbitals of the PtL_2 fragment have the potential to form radial and tangential MOs which are entirely equivalent to those formed by $M(CO)_3$ fragments in an analogous polyhedral cluster. The bonding MOs which are derived from the p_y orbitals however are not sufficiently stable for electron occupation as a result of the large d–p promotion energy of platinum [9]. Consequently the bonding in platinum clusters is dominated by the symmetries and

energies of the skeletal molecular orbitals derived from hy(s-z) and hy(xz) frontier orbitals. For all clusters the hy(s-z) orbitals give rise to one totally symmetric molecular orbital which is bonding. The number of bonding tangential skeletal molecular orbitals obtained from the hy(xz) orbitals depends markedly on the conformation adopted by the individual PtL_2 fragments relative to the principal axis of the polyhedron. This contrasts with the situation which pertains for clusters derived from conical fragments where the nature of the tangential MOs is independent of the conformation of the fragments. As discussed in our previous paper [4], consideration of alternative latitudinal and longitudinal conformers (vide infra) leads to a considerable simplification of the quantum mechanical problem since it allows the synthesis of first order perturbation theory arguments with the elegant Tensor Surface Harmonic Theory of Stone [10] to give a coherent picture of the MOs in platinum clusters.

We consider first the case of tetrahedral clusters derived from four PtL_2 fragments and extend our analysis summarised previously [4]. The bonding in such tetrahedral $Pt_4(PH_3)_8$ clusters may be usefully analysed by considering the two alternative conformers **1** and **2** denoted as latitudinal and longitudinal respectively, both of which have D_{2d} symmetry.

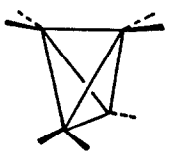

(1)

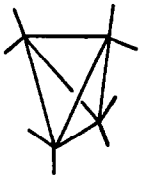

(2)

In the case of a tetrahedral cluster derived from conical ML_3 fragments, the eight tangential MOs are t_2 (bonding), e (approximately non-bonding) and t_1 (antibonding). The replacement of the conical fragments by angular $Pt(PH_3)_2$ fragments with widely separated hy(xz) and p_y orbitals leads to the orbital splitting patterns illustrated in Fig. 2.

The molecular orbitals derived from hy(xz) for the alternative conformers **1** and **2** when added together correspond to the tangential skeletal molecular orbitals for a tetrahedron derived from conical fragments i.e. $t_2 = e + b_2$; $e = b_1 + a_1$ and $t_2 = a_2 + e$. Although both conformers have a total of four molecular orbitals derived from the hy(xz) orbitals, the distribution between bonding and antibonding orbitals differs for the two conformers. In particular, the latitudinal conformer has an e bonding set and a b_1 non-bonding orbital derived from the hy(xz) orbitals, whereas the longitudinal conformer has only one b_2 bonding molecular orbital in addition to an a_1 non-bonding orbital (see Fig. 2).

The radial bonding and antibonding molecular orbitals derived from hy(s-z) are almost independent of the conformation of the $Pt(PH_3)_2$ fragments and in each case there is a single bonding component of a_1 symmetry. In fact the energies of this a_1 orbital vary slightly with conformation as shown in Fig. 2. This can be interpreted in terms of mixing between a_1 orbitals derived from hy(s-z) and hy(xz) in the case of the longitudinal conformer.

It can be readily appreciated from the calculations that the maximum skeletal

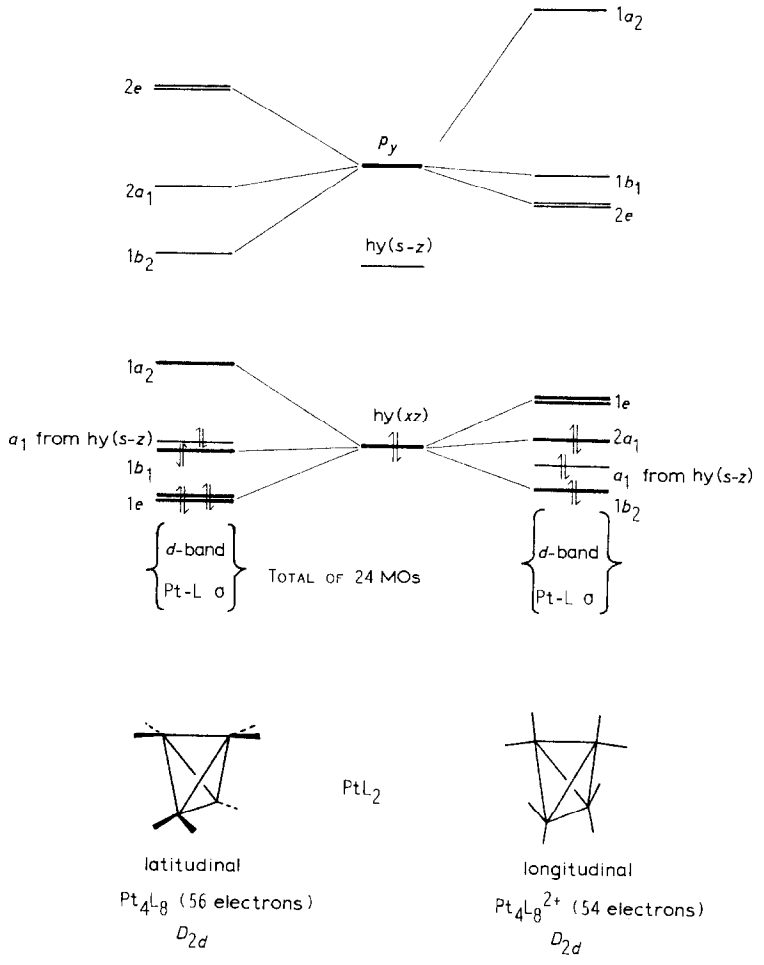

Fig. 2. Cluster MOs for $Pt_4(PH_3)_8$ in latitudinal and longitudinal conformations.

bonding will be achieved for the latitudinal conformer when the total electron count is 56, whereas for the longitudinal conformer the preferred electron count is 54. Since the former has an additional skeletal electron pair (four as opposed to three) then it can be expected to be more favourable. This conformational preference is reinforced by the greater overlap integrals between the hy(xz) orbitals in the latitudinal conformer, because of the greater σ-component to the overlap in this case, and furthermore by substantial steric repulsions between the PH_3 ligands in the longitudinal conformer of $Pt_4(PH_3)_8$. (In the context of the Extended Hückel calculations reported here such steric effects are represented by four electron destabilising interactions between filled ligand orbitals).

It is likely that these unfavourable effects could only be mitigated if two adjacent terminal ligands in **2** are replaced by a bridging group such as a phosphido group, or alternatively two pairs of adjacent ligands could be replaced by a chelating diphosphine such as dppm which readily bridges metal–metal bonds. Two possible structures consistent with these predictions are illustrated in **3**.

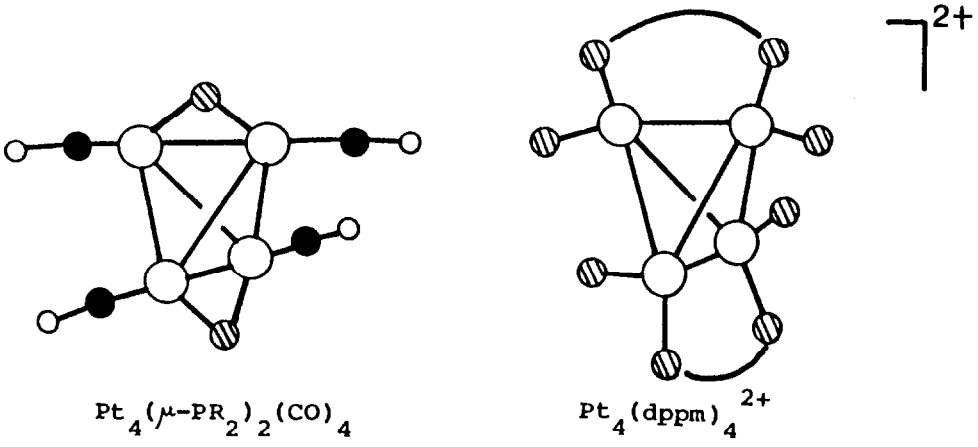

(3)

The analysis of the bonding in $Pt_4(PH_3)_8$ presented so far has implied that the p_y orbitals of the $Pt(PH_3)_2$ fragments play no effective role in the bonding as a consequence of their high-lying nature. A more detailed analysis of the calculations however suggests that the p_y orbitals play an important secondary bonding role. In the latitudinal conformer **1**, the $1e$ set derived from the hy(xz) orbitals mixes with an antibonding e set from the d band. The resulting eight electron destabilising interactions are mitigated by a mixing in of the e set derived from the p_y orbitals. This mixing accounts for the final, approximately non-bonding, form of the $1e$ orbitals (see Fig. 1). One component of this $1e$ set is illustrated in **4**.

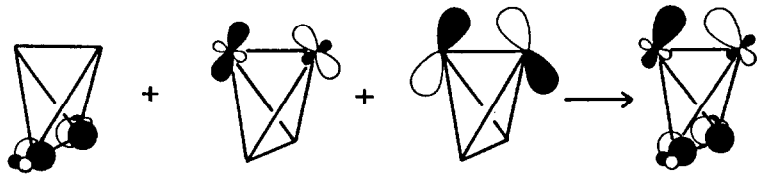

(4)

Although the e set derived from the hy(xz) orbitals can be stabilised in this way, the $1b_1$ and $1a_2$ orbitals which are also derived from hy(xz) orbitals cannot be stabilised by the other combination of p_y orbitals since these are of the wrong symmetry ($1b_2$ and $2a_1$ in Fig. 2) and these latter orbitals have no influence on the bonding.

In the case of the longitudinal conformer **2**, the antibonding combination of hy(xz) orbitals, $1e$ in Fig. 2, interacts much less weakly with the orbitals in the d band but is also much less strongly stabilised by interaction with the $2e$ set derived from the p_y orbitals so that its occupation is unfavourable. As in the case of the latitudinal conformer the occupied $1b_2$ and $2a_1$ orbitals derived from hy(xz) are of the incorrect symmetry to be stabilised by mixing with the other MOs derived from p_y ($1b_1$ and $1a_2$ in Fig. 2).

The net result is that the platinum p_y orbitals are more effective in stabilising the occupied cluster bonding MOs in the case of the latitudinal conformer which contributes to the conformational preference described above.

Even in the case of the latitudinal conformer, the fragment p_y orbitals play a relatively minor part in the bonding. These orbitals are ideally disposed to interact with bridging ligands and it can be further anticipated that $Pt_4(PH_3)_4H_4(\mu\text{-}H)_4$ will be more stable than the isoelectronic $Pt_4(PH_3)_8$ species. As expected MO schemes for the latitudinal and longitudinal conformers of $Pt_4(PH_3)_4^{4-}$ are very similar to those of the corresponding conformers of $Pt_4(PH_3)_8$, with the latitudinal conformer being the more favourable.

Two arrangements of the four bridging hydrogen ligands, both of which retain the S_4 symmetry, can be envisaged. Both of these structures have been observed in tetrahedral clusters, examples being $Os_4(CO)_{12}(\mu_2\text{-}H)_4$ and $Co_4Cp_4(\mu_3\text{-}H)_4$ respectively. The calculations suggest that the introduction of four bridging ligands in either geometry markedly reinforces the conformational preference of the terminal ligands apparent in $Pt_4(PH_3)_8$ so that only the latitudinal conformers of $Pt_4(PH_3)_4H_4(\mu_3\text{-}H)_4$ (**5**) and $Pt_4(PH_3)_4H_4(\mu_2\text{-}H)_4$ (**6**) will be considered further here.

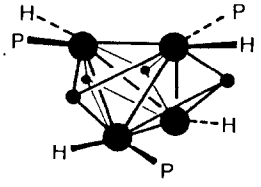

(5)

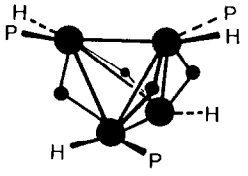

(6)

The MO interaction diagram for $Pt_4(PH_3)_4H_4(\mu_3\text{-}H)_4$ is illustrated in Fig. 3. The 1*s* orbitals of the bridging hydrogen ligands give rise to $a + b + e$ combinations in S_4. As discussed above and illustrated in **4** for $Pt_4(PH_3)_8$ there is extensive mixing between the three orbitals of *e* symmetry derived from *d*, hy(*xz*) and p_y orbitals. An analogous arrangement of three *e* sets is found for $Pt_4(PH_3)_4^{4-}$. The lowest, most bonding *e* level, one component of which is illustrated in **7**, is ideally oriented to interact with face bridging ligands, giving the strongly bonding 1*e* set in $Pt_4(PH_3)_4H_4(\mu_3\text{-}H)_4$.

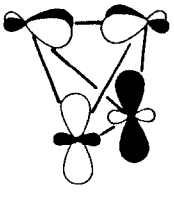

(7)

The upper component of this cluster-bridging ligand interaction (2*e* in Fig. 3) is extensively stabilised by mixing with the upper two *e* levels of $Pt_4(PH_3)_4H_4^{4-}$ so that occupation of 1*e* and 2*e* therefore leads to a net bonding interaction. Furthermore the *a* and *b* combinations of hydrogen 1*s* orbitals also enter into net bonding

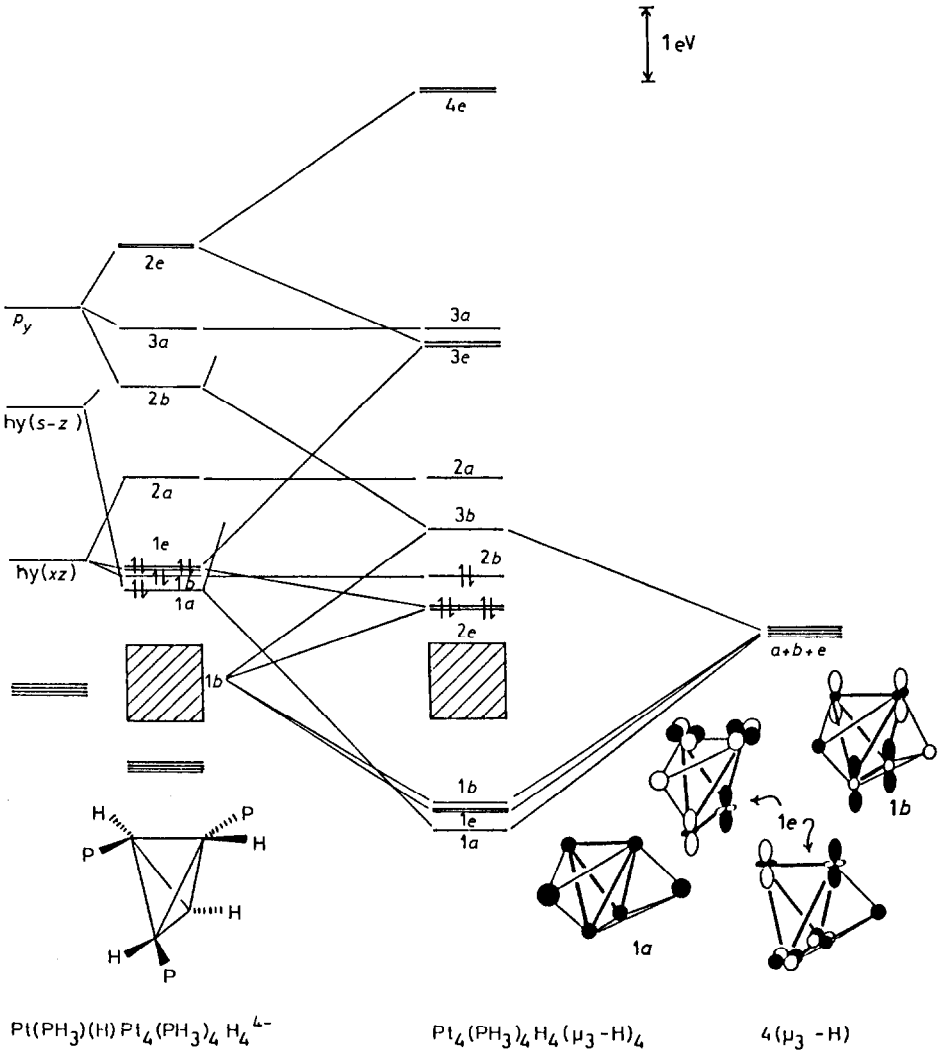

Fig. 3. MO interaction diagram for $Pt_4(PH_3)_4^{4-}$ in the latitudinal conformation with four face bridging protons.

interactions. The *a* combination interacts with the *a* combination of fragment hy(*s*-*z*) orbitals to give the strongly bonding 1*a* orbital whilst the *b* combination interacts with an orbital of *b* symmetry from the *d* band forming the 1*b* level in Fig. 3. That the *b* combination does not overlap significantly with the *b* combination of hy(*xz*) orbitals in $Pt_4(PH_3)_4H_4^{4-}$ is easy to see because the latter is not very favourably oriented for such overlap.

The interaction of four edge bridging hydrogen ligands with the cluster is illustrated in Fig. 4. The *e* and *b* combinations of bridging ligand orbitals interact with appropriate combinations of fragment *d* orbitals to give bonding 1*b* and 1*e* levels. As for the case of the face bridging ligands the *a* combination of hydrogen 1*s*

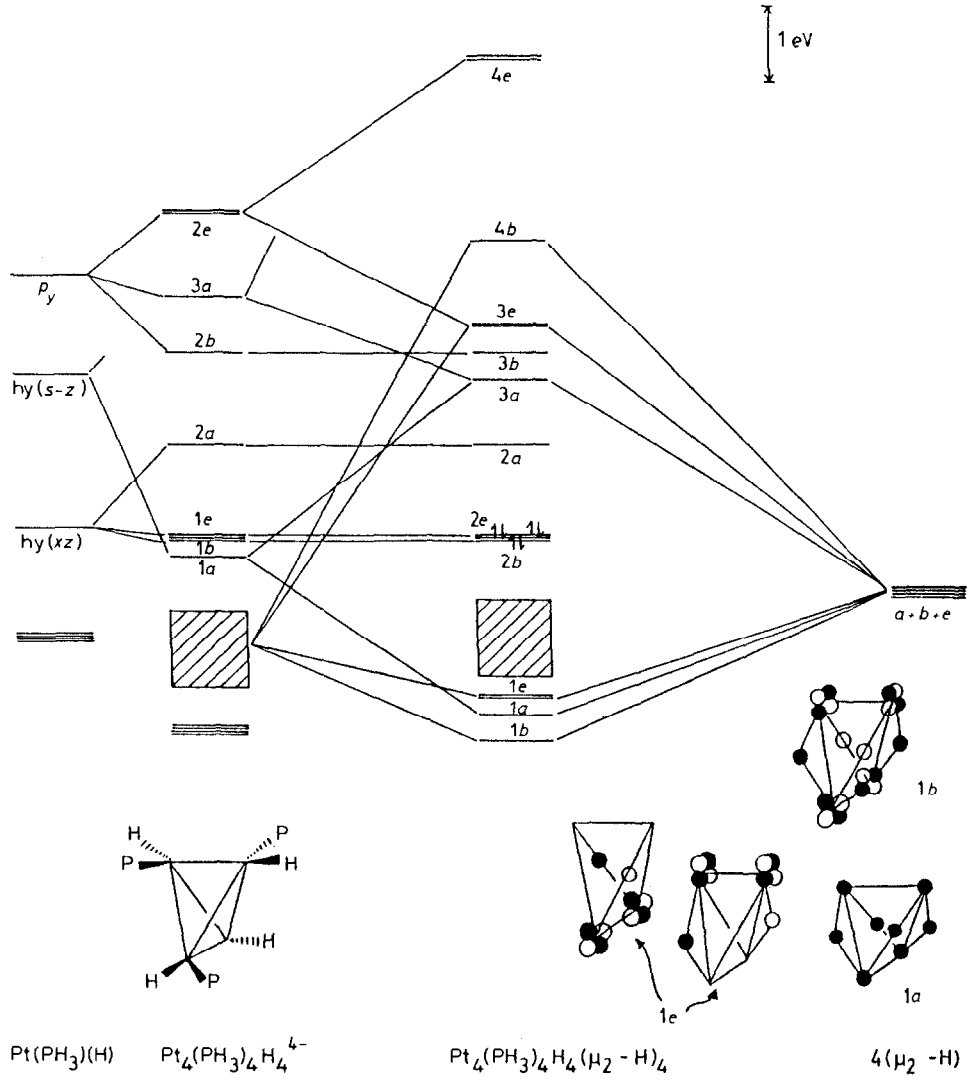

Fig. 4. MO interaction diagram for $Pt_4(PH_3)_4^{4-}$ in the latitudinal conformation with four edge bridging protons.

orbitals interacts with the *a* combination of fragment hy(*s*-*z*) orbitals to give the bonding 1*a* level. The orientation of the cluster orbitals is such that the overlap with the edge bridging ligands is less favourable than that with the face bridging ligands. The calculations suggest that the face bridged isomer of $Pt_4(PH_3)_4H_4(\mu\text{-}H)_4$ is 1.4 eV more stable.

It has been previously observed however [11] that one of the deficiencies of the Extended Hückel method is that it tends to over-estimate the stability of triply- over doubly-bridged hydrogen ligands. This suggests that merely comparing the relative energies of **5** and **6** may not be sufficient to determine the preferred geometry. The computed Mulliken overlap populations for the latitudinal conformers of

$Pt_4(PH_3)_4^{4-}$, $Pt_4(PH_3)_4(\mu_3\text{-}H)_4$ and $Pt_4(PH_3)_4H_4(\mu_2\text{-}H)_4$ which are reproduced in **8** suggest a substantial asymmetry in the lengths of the metal–metal bonds, particularly for the first two compounds.

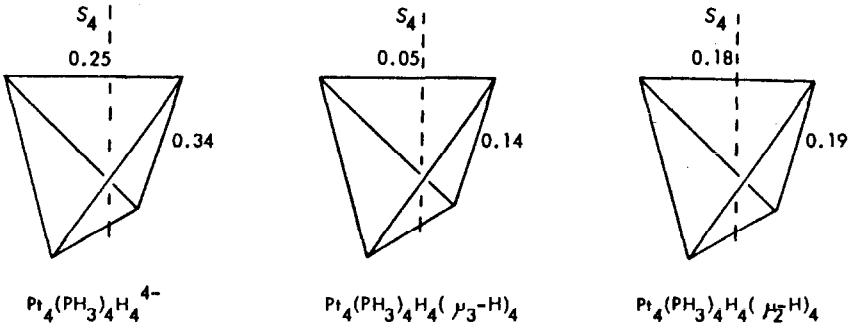

(8)

This asymmetry can be attributed to the loss of spherical symmetry in the tangential molecular orbitals which results from the fact that $Pt(PH_3)(H)$ presents only a single hy(xz) orbital for tangential cluster bonding. Indeed the nodal characteristics of the highest-lying $1b$ molecular orbital derived from hy(xz) and illustrated in **9** are such that it is antibonding along the Pt–Pt bonds bisected by the S_4 axis. In the μ_3-hydrido cluster this asymmetry is more pronounced because this molecular orbital retains its metal character whereas the lower lying $1a$ and $1e$ orbitals derived from hy(xz) interact with the face bridging hydrogen ligands and become more delocalised.

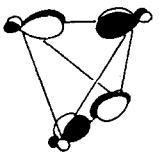

(9)

The cluster $Pt_4(PPr^i{}_2Ph)_4H_8$ has been reported by Spencer [2]. The X-ray crystal structure revealed a central Pt_4P_4 core with S_4 symmetry with four short Pt–Pt distances (mean 2.78 Å) and two longer distances (mean 3.08 Å). The P–Pt–P angles are very close to those calculated for the latitudinal conformer of $Pt_4(PH_3)_4H_4^{4-}$. Although the hydrogen atoms were not located the arrangement of the phosphorus atoms and the asymmetry in the platinum–platinum bond lengths enables it to be confidently predicted that the structure is based on the latitudinal conformer of $Pt_4(PH_3)_4H_4$ with four face bridging hydrogen ligands but this could only be confirmed unambiguously by neutron diffraction experiments.

The structures of some other related isoelectronic tetrahedral clusters have been recently reported. Fryzuk [12] has recently suggested on the basis of NMR evidence that $Rh_4[(MeO)_2PCH_2CH_2P(OMe)_2]_4H_4$ has a tetrahedral Rh_4P_8 core with four triply bridging hydride ligands. Also Muetterties et al. [13] have reported the

structure of $Rh_4(COD)_4H_4$. The central Rh_4 core has idealised D_{2d} symmetry with two long (mean 2.971 Å) and four short (mean 2.802 Å) edges. Although the bridging hydride ligands were located there were, not unexpectedly for a room temperature X-ray data set, large standard deviations in the Rh–H bond lengths and it is therefore difficult to decide unambiguously whether the hydrides are edge or face bridging. Thus final confirmation of the structure of one of these species must await definitive neutron diffraction studies.

We now consider two alternative geometries for Pt_4L_4 clusters, **10** and **11**, which may be formally derived from the above latitudinal and longitudinal conformers of Pt_4L_8 respectively, by removal of four L ligands.

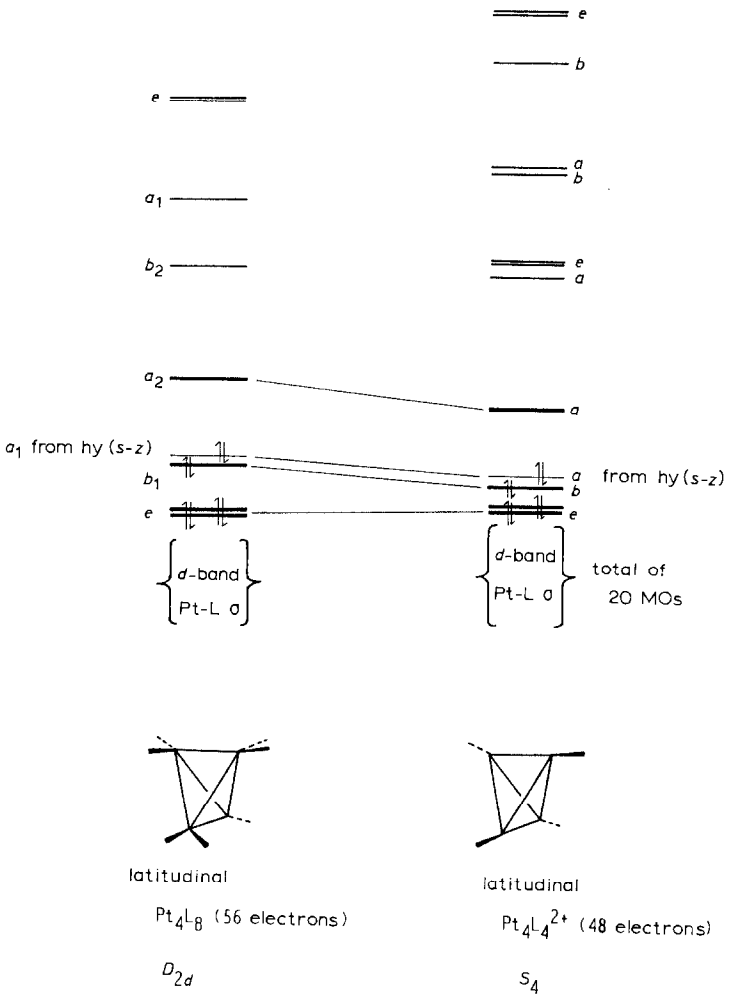

Fig. 5. A comparison of the cluster MOs for the latitudinal conformations of $Pt_4(PH_3)_8$ and $Pt_4(PH_3)_4^{2+}$. The unoccupied antibonding a_2 orbital derived from hy(xz) in the former cluster correlates with a similar orbital in the latter cluster, so that the latter cluster is characterised by eight fewer electrons corresponding to the loss of four Pt–L bonding MOs.

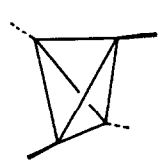

(10)

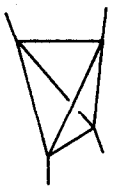

(11)

The MO scheme for the latitudinal conformer of $Pt_4(PH_3)_4$ (**10**), which has S_4 symmetry, is closely related to that of the corresponding conformer of $Pt_4(PH_3)_8$ (**1**), as shown in Fig. 5. The descendents of the metal–metal bonding $a_1\{hy(s\text{-}z)\}$, b_1 and e orbitals are occupied, whilst the antibonding a_2 orbital in **1** correlates with an a orbital in **10** which remains strongly antibonding and unoccupied. The form of this orbital is illustrated in **12**.

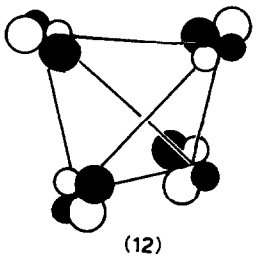

(12)

A Pt_4L_4 cluster with the geometry **10** is therefore expected to have an electron count of 48 - eight fewer than the latitudinal conformer of Pt_4L_8 (**1**), corresponding to the loss of four M–L bonding MOs.

In the case of the longitudinal conformer of $Pt_4(PH_3)_4$ (**11**), however, a significant difference arises. As discussed above, the overlap integrals between the hy(xz) orbitals in the longitudinal conformer of Pt_4L_8 (**2**), are smaller than those in the latitudinal conformer **1** because of the larger σ-component to the overlap in the latter. Loss of four L ligands from **2** to generate **11** further reduces the overlap between the descendents of the hy(xz) orbitals so that the antibonding e set in **2** correlates with a weakly antibonding e set at the top of the d band in **11** and is thus available for occupation, becoming the HOMO of the cluster. Thus in going from Pt_4L_8 (**2**) to Pt_4L_4 (**11**), there is expected to be a net loss of four electrons, corresponding to the loss of four M–L bonding MOs, but occupation of two additional metal d MOs. Thus the electron count for **11** is expected to be 50, two more than for **10**. The predicted electron counts are summarised in Table 1.

The antibonding nature of the e set forming the HOMOs in $Pt_4(PH_3)_4^{2-}$ (**11**), may be reduced even further by distortion of the phosphine ligands such that they point towards the centroid of the Pt_4P_4 tetrahedron. Such a distortion stabilises the $Pt_4(PH_3)_4^{2-}$ cluster by 1.3 eV but does not change the predicted electron count. The bonding in such a $Pt_4(PH_3)_4^{2-}$ cluster has been discussed by us elsewhere [14] as part of a general analysis of the bonding in clusters derived from $M(PH_3)$ fragments. The way in which such a cluster was stabilised by the introduction of two bridging hydrogen ligands was also discussed and the MOs of the resulting $Pt_4(PH_3)_4H_2$ cluster used to rationalise the electronic and structural features of $Pt_4(PBu^t_3)_4H_2$ cluster as reported by Spencer [2].

TABLE 1

PREDICTED ELECTRON COUNTS IN TETRAHEDRAL PLATINUM CLUSTERS

Latitudinal		Longitudinal	
Electron count	Parent cluster	Electron count	Parent cluster
56	$Pt_4(PH_3)_8$	54	$Pt_4(PH_3)_8^{2+}$
48	$Pt_4(PH_3)_4$	50	$Pt_4(PH_3)_4^{2-}$

It is of interest to explore the effect on $Pt_4(PH_3)_4$ (**10**), of introducing two bridging hydrogen ligands. Calculations show that, as might be expected from the discussion presented above for $Pt_4(PH_3)_4H_4^{4-}$ and elsewhere for $Pt_4(PH_3)_4^{2-}$ [14] that this has a stabilising effect on the cluster, without introducing any additional occupied orbitals. Thus a 48 electron cluster results, corresponding to the species $Pt_4(PH_3)_4H_2^{2+}$. Two alternative geometries, with face bridging and edge bridging hydride ligands are illustrated in **13** and **14** respectively.

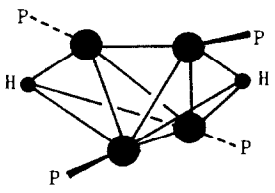

(13)

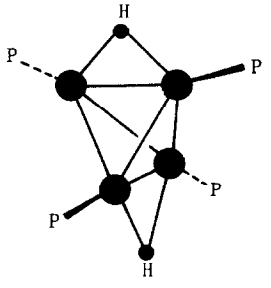

(14)

In each case the bridging hydrogen 1*s* orbitals give rise to linear combinations of *a* and *b* symmetry. The former interacts with and stabilises the *a* combination of fragment hy(*s*-*z*) orbitals, whilst the latter interacts with and stabilises an appropriate combination from the *d* band. The calculations show that the energies of the two resulting clusters are very similar, with the edge bridged cluster $Pt_4(PH_3)_4(\mu_2\text{-}H)_2^{2+}$ lying some 0.05 eV lower in energy. As discussed above however, a more reliable prediction of the location of the bridging hydride ligands may be made using the computed Mulliken overlap populations. These are shown in **15** and **16** for $Pt_4(PH_3)_4(\mu_3\text{-}H)_2^{2+}$ and $Pt_4(PH_3)_4(\mu_2\text{-}H)_2^{2+}$, respectively.

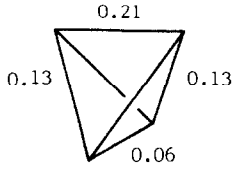

(15)

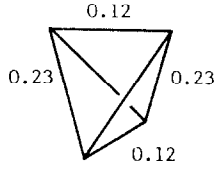

(16)

In **16** the hydride ligands bridge the two edges of the Pt_4 tetrahedron bisected by the S_4 axis such that the metal–metal bonding electron density along these edges is delocalised onto the ligands giving a pattern of two long and four short bonds.

Similar arguments may be applied to the case of the face bridged cluster where there are expected to be three different sets of metal–metal bond lengths.

The crystal structure of $Pt_4(PBu^t_3)_4H_2^{2+}$ has been reported by Spencer [3]. The structure of this 48-electron cluster shows an S_4 distorted Pt_4 core as expected from the above calculations with two long (mean 2.84 Å) and four short (mean 2.61 Å) Pt–Pt bonds, but the hydride ligands were not located. The calculations suggest that the two hydride ligands bridge opposite edges of the tetrahedron but this could only be confirmed by neutron diffraction experiments.

It is of interest to compare the clusters $Pt_4(PH_3)_4H_4(\mu_3\text{-}H)_4$ (56 electrons) and $Pt_4(PH_3)_4(\mu_2\text{-}H)_2^{2+}$ (48 electrons) which both have Pt_4P_4 cores of S_4 symmetry. The computed overlap populations reproduced in **8** and **16** respectively indicate that the metal–metal overlap is much larger in the latter case and this is reflected in the metal–metal bond lengths of $Pt_4(PPr^i_2Ph)_4H_8$ which are approximately 0.25 Å longer than those in $Pt_4(PBu^t_3)_4H_2^{2+}$.

We now consider the bonding in some trigonal bipyramidal clusters. For the $Pt_5(PH_3)_{10}$ cluster we consider the latitudinal and longitudinal conformers illustrated in Fig. 6. The latitudinal conformer has three bonding cluster MOs whilst the longitudinal conformer has four.

Therefore by analogy with the previous analysis the latter, corresponding to a stoichiometry $Pt_5(PH_3)_{10}^{2+}$ and a 68-electron count is expected to be the more stable. No such cluster has been observed however but this is not perhaps surprising in view of the substantial steric crowding which could be present.

Although Pt_5L_{10} clusters are rather sterically hindered this problem is overcome if the equatorial groups are replaced by PtL. Three of the possible conformations of the axial PtL_2 groups are illustrated in **17–19**, looking down onto the Pt_3L_3 plane.

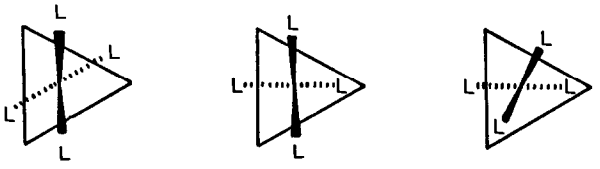

(17) (18) (19)

The interaction between the $Pt_3(PH_3)_3$ and the capping $Pt(PH_3)_2$ groups is almost independent of the orientation of the latter and the calculations show that the three conformers of $Pt_5(PH_3)_7$ have very similar energies with **17** being marginally the most stable.

The interaction diagram for the capping of a $Pt_3(PH_3)_3$ triangle with $Pt(PH_3)_2$ groups to give $Pt_5(PH_3)_7$ in conformation **17** is shown in Fig. 7.The only orbitals from the *d* band of the triangle which overlap effectively with the frontier orbitals of the capping fragments are the bonding $1a_1'$ and antibonding $1e'$ combination of $Pt_3(PH_3)_3$ d_{z^2} orbitals. The former interacts with the in-phase combination of $Pt(PH_3)_2$ hy(*s*-*z*) orbitals giving $1a$ in $Pt_5(PH_3)_7$ whilst both components of the latter $1e'$ set are stabilised by interaction with $Pt(PH_3)_2$ hy(*xz*) orbitals to give bonding and antibonding $4a$ and $5a$ levels. The out-of-phase combination of $Pt(PH_3)_2$ hy(*s*-*z*) orbitals interacts with $1a_2''$ in $Pt_3(PH_3)_3$ derived from $Pt(PH_3)p_z$ orbitals to give the $6a$ level in $Pt_5(PH_3)_7$.

If the $4a$, $5a$ and $6a$ levels are assumed to be unoccupied then the total electron

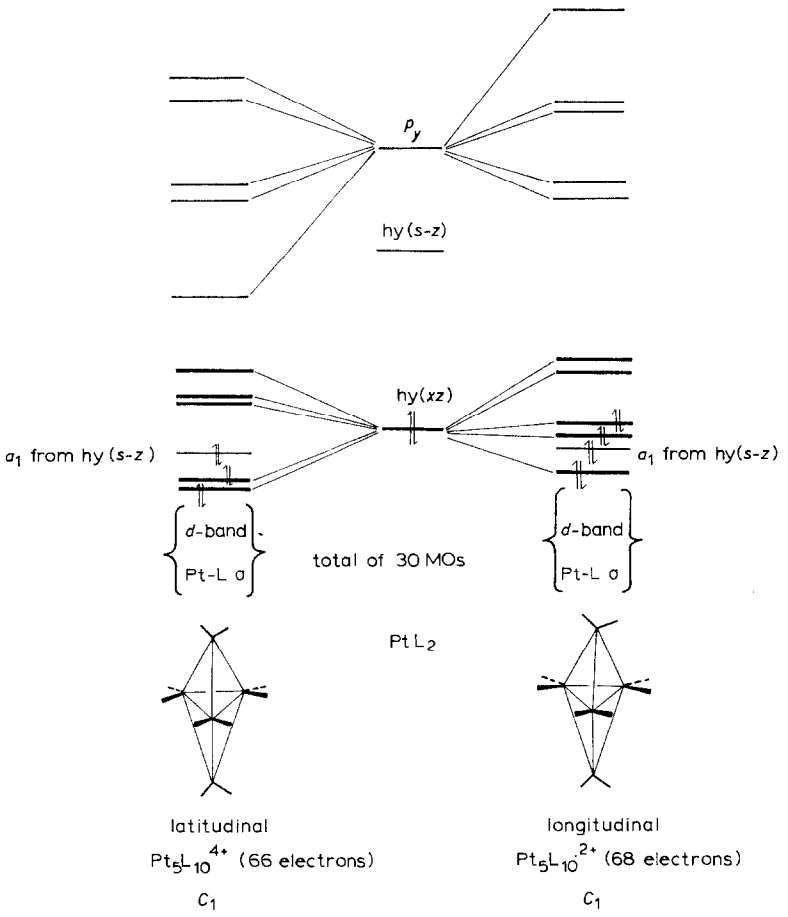

Fig. 6. Cluster MOs for $Pt_5(PH_3)_{10}$ in latitudinal and longitudinal conformations.

count is 62, corresponding to the stoichiometry $Pt_5(PH_3)_7^{2+}$ or $Pt_5(PH_3)_5H_2$. We have shown previously however that such clusters are markedly stabilised by the presence of bridging hydride ligands. It is therefore reasonable to suppose that occupation of the weakly antibonding $4a$ and $5a$ levels together with the introduction of four such ligands will lead to a more stable 66 electron $Pt_5(PH_3)_5H_2(\mu\text{-H})_4$ cluster. In such a cluster however the LUMO is not too high-lying and is ideally disposed to interact with bridging ligands suggesting the existence of a second series of pentanuclear platinum clusters, $Pt_5(PR_3)_5H_2(\mu\text{-H})_6$, with a 68 electron count, and we will analyse the bonding in such clusters in more detail.

The energy level diagram for $Pt_5(PH_3)_5H_2^{6-}$, in a conformation corresponding to **17** is shown in Fig. 8 and as expected is very similar to that of $Pt_5(PH_3)_7$. On symmetry grounds it is reasonable to place the six bridging hydrogen ligands along either the six axial Pt–Pt bonds, or over the six faces of the polyhedron. The interaction diagram for six edge bridging hydrogen ligands is shown in Fig. 8. The six linear combinations of hydrogen $1s$ orbitals each find a match in orbitals from the d band whilst the $4a$, $5a$ and in particular $6a$ orbitals are stabilised by

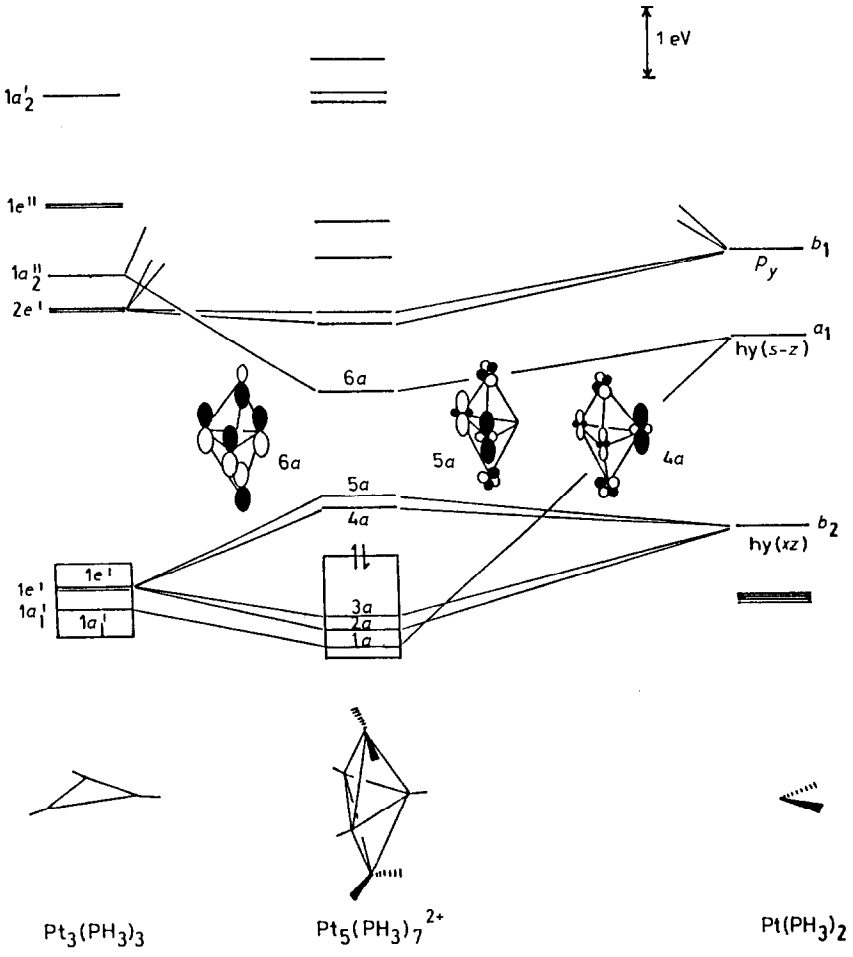

Fig. 7. MO interaction diagram for $Pt_3(PH_3)_3$ with two capping $Pt(PH_3)_2$ fragments.

interaction with the antibonding components of the first order metal–hydrogen interaction.

As shown in Fig. 9 a very similar energy level scheme pertains to the cluster with face bridging hydrogen ligands. The calculations indicate that the face bridged structure is slightly more stable, by 0.4 eV, but as has been shown elsewhere [11], such small energy differences in Extended Hückel calculations are not a reliable guide to the mode of hydrogen bridging.

It is more instructive to examine the computed Mulliken overlap populations. For the parent $Pt_5(PH_3)_5H_2^{6-}$ cluster these are shown in **20**. The overlap populations along the axial bonds are larger than those along the equatorial bonds, primarily as a consequence of the nodal characteristics of the $6a$ orbital (see Fig. 8) which is more strongly bonding along these edges. The tendency of the $Pt(PH_3)(H)$ fragments to slip towards the edge of the Pt_3 triangle to which they are parallel in order to maximise the overlap of the hy(xz) orbital with the appropriate component of the $1e'$ set is also apparent from these overlap populations.

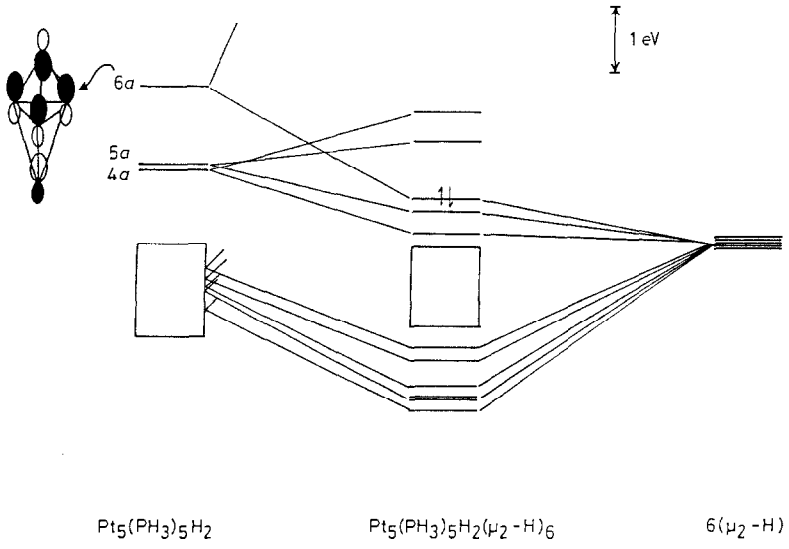

Fig. 8. MO interaction diagram for $Pt_5(PH_3)_5H_2^{6-}$ with six edge-bridging protons.

Six edge bridging hydrogen ligands interact with appropriate orbitals from the *d* band which are in phase along the axial edges, with a consequent diminution in the direct axial metal–metal bonding but will have little effect on the equatorial bonds. This is borne out by the computed overlap populations for $Pt_5(PH_3)_5H_2(\mu_2\text{-}H)_6$ reproduced in **21**. The slip distortion of the $Pt(PH_3)(H)$ fragments is expected to be

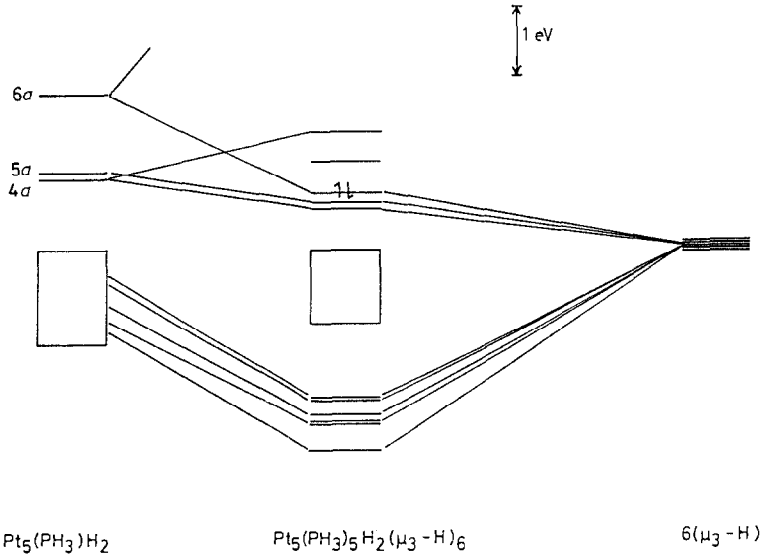

Fig. 9. MO interaction diagram for $Pt_5(PH_3)_5H_2^{6-}$ with six face-bridging protons.

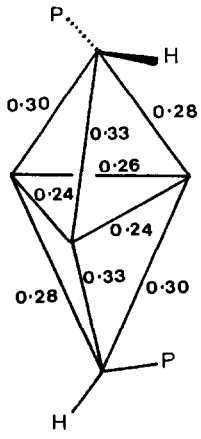

(20)

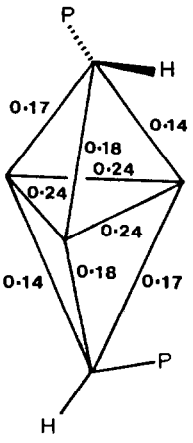

(21)

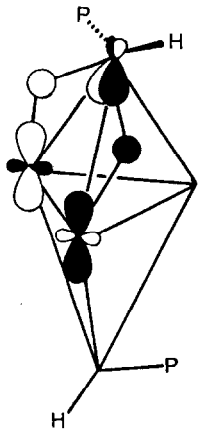

(22)

enhanced by the presence of the edge bridging hydride ligands, as illustrated for one component of the bonding interaction in **22**.

In the case of the face bridging hydrogen ligands their primary interaction is with orbitals from the *d* band which are in phase over a face, which will lead to a diminution in both axial and equatorial metal–metal bonding. Furthermore since the hy(xz) orbitals and the 1e' set are not in phase over the faces then the tendency towards slipping in order to maximise this interaction will be reduced. The computed overlap populations for $Pt_5(PH_3)_5H_2(\mu_3\text{-}H)_6$ shown in **23** are in accord with this analysis and suggest that slipping towards a vertex is in fact more probable than slipping towards an edge of the Pt_3 triangle.

The crystal structure of one such pentanuclear cluster compound, $Pt_5(PBu^t_2Ph)_5\text{-}H_8$ has recently been reported by Spencer et al. [1]. The molecule consists of a distorted trigonal bipyramidal Pt_5P_5 core but no direct evidence for the location of the hydride ligands was obtained. The axial phosphines deviate appreciably from

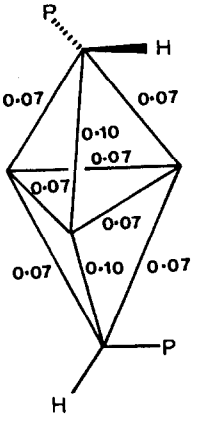

(23)

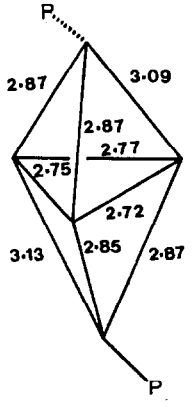

(24)

the axial Pt–Pt vector indicative of the presence of two axial $Pt(PR_3)(H)$ groups. Furthermore the crystal structure indicates that each of the axial Pt–P vectors is parallel to an edge of the Pt_3 equatorial triangle and that each apical platinum atom slips towards the appropriate edge of the triangle. The close correspondence between the observed bond lengths shown in **24** and the overlap populations shown in **23** lead us to suggest that the six bridging hydrogen ligands are located along the six axial metal–metal bonds rather than over the faces.

Neutron diffraction studies on this cluster would be most interesting to check the validity of this prediction.

Appendix

All the calculations were performed using the Extended Hückel method with the relevant orbital parameters given in Tables 2a and 2b. All the parameters conform to those which have been used to give reliable conclusions for organo-transition metal compounds [17]. The off-diagonal terms in the Extended Hückel calculations were estimated from the expression $H_{ij} = 1.75S_{ij}(H_{ii} + H_{jj})/2$ [18].

The following bond lengths were used for the calculations: Pt–Pt 2.70, Pt–P 2.27, P–H 1.42, PtH(terminal) 1.70, Pt–H(μ_2-bridging) 1.80, Pt–H(μ_3-bridging) 1.80 Å. The calculations were performed on the ICL2988 computer at the South-West Universities Regional Computer Centre using the programs ICON8 and FMO [19].

Conclusions

The theoretical analysis presented here has demonstrated that it is possible to account for the structures of, and total electron counts in, clusters containing non-conical PtL_2 fragments within the framework of the Polyhedral Skeletal Electron Pair Theory. The non-conical nature of the fragment means that it generally has a marked conformational preference in its cluster compounds. There was found

TABLE 2a

PARAMETERS FOR NON-METAL ATOMS

Atom	Orbital	Slater exponent	H_{ii} (eV)	Reference
H	1*s*	1.30	−13.60	5
P	3*s*	1.60	−18.60	15
	3*p*	1.60	−14.00	15

TABLE 2b

PARAMETERS FOR PLATINUM ATOM [16]

Orbital	H_{ii} (eV)	ζ_1	c_1	ζ_2	c_2
6*s*	−9.80	2.550			
6*p*	−5.35	2.550			
5*d*	−10.61	6.010	0.6330	2.700	0.5510

to be good agreement between the observed conformations in tetra- and penta-nuclear clusters and that which was calculated to be the most stable in each case.

The metal–metal bonding between ML_2 fragments in a cluster appears to be much less effective than that between conical ML_3 fragments. Consequently the former fragments are generally associated with bridging ligands such as hydride. The calculations reported here have demonstrated how these ligands stabilise the cluster and also enabled their coordination mode (i.e. edge or face bridging) to be predicted since this cannot usually be determined crystallographically.

The introduction of PtL fragments into some of the clusters leads to a further flexibility in electron count. In such fragments the single terminal ligand has a considerable freedom of movement around the platinum atom and the rehybridisation of orbitals which accompanies such geometric changes can lead to alternative electron counts being favoured.

Acknowledgements

Dr. D.M.P. Mingos is thanked for useful comments and Miss Julie Harris for assistance with the computing.

References

1 D. Gregson, J.A.K. Howard, M. Murray and J.L. Spencer, J. Chem. Soc., Chem. Commun., (1981) 716.
2 P.W. Frost, J.A.K. Howard, J.L. Spencer and D.G. Turner, J. Chem. Soc., Chem. Commun., (1981) 1104.
3 R.J. Goodfellow, E.M. Hamon, J.A.K. Howard, J.L. Spencer and D.G. Turner, J. Chem. Soc., Chem. Commun., (1984) 1604.
4 D.G. Evans and D.M.P. Mingos, J. Organomet. Chem., 240 (1982) 321.
5 R. Hoffmann, J. Chem. Phys., 39 (1963) 1397.
6 D.M.P. Mingos, Adv. Organomet. Chem., 15 (1977) 1.
7 M. Elian, M.M.L. Chen, R. Hoffmann and D.M.P. Mingos, Inorg. Chem., 15 (1976) 1148.
8 M. Elian and R. Hoffmann, Inorg. Chem., 14 (1975) 1058.
9 F.G.A. Stone, Inorg. Chim. Acta, 50 (1981) 33.
10 A.J. Stone, Inorg. Chem., 20 (1981) 563.
11 R. Hoffmann, B.E.R. Schilling, R. Bau, H.D. Kaesz and D.M.P. Mingos, J. Amer. Chem. Soc., 100 (1978) 6088.
12 M.D. Fryzuk, Organometallics, 1 (1982) 408.
13 M. Kulzick, R.T. Price and E.L. Muetterties, Organometallics, in press.
14 D.G. Evans and D.M.P. Mingos, J. Organomet. Chem., 232 (1982) 171.
15 E. Clementi, J. Chem. Phys., 40 (1964) 1944.
16 F.A. Cotton and C.B. Harris, Inorg. Chem., 6 (1967) 369.
17 R. Hoffmann, Angew. Chem. Int. Ed. Engl., 21 (1982) 711 and references therein.
18 R. Hoffmann and W.N. Lipscomb, J. Chem. Phys., 36 (1962) 2179.
19 J. Howell, A. Rossi, D. Wallace, K. Haraki and R. Hoffmann, Quantum Chemistry Program Exchange, 10 (1977) 344.